Computation of the High Temperature Coulomb Density Matrix in Periodic Boundary Conditions

B. Militzer

Department of Earth and Planetary Science and Department of Astronomy, University of California, Berkeley, CA 94720

Abstract

The high temperature many-body density matrix is fundamental to path integral computation. The pair approximation, where the interaction part is written as a product of pair density matrices, is commonly used and is accurate to order τ^2, where τ is the step size in the imaginary time. Here we present a method for systems with Coulomb interactions in periodic boundary conditions that consistently treats the all interactions with the same level of accuracy. It is shown that this leads to a more accurate high temperature solution of the Bloch equation. The method is applied to many-body simulation and tests for the isolated hydrogen atom and molecule are presented.

Key words: Path integral Monte Carlo, many-body simulations
PACS: 71.10.-w, 71.15.Pd,, 71.15.Dx, 61.20.Ja

1. Introduction

Quantum Monte Carlo (QMC) methods are frequently used to study interacting many-body systems in different fields of physics and chemistry when a high degree of accuracy is needed [1]. The description of correlation effects combined with favorable scaling properties of N^3 or better (N is the number of particles) make these techniques effective in many applications. Path integral Monte Carlo (PIMC) is unique among other QMC methods because it can describe quantum systems at *finite temperature* [2, 3, 4, 5, 6]. The method is based on the thermal density matrix that characterizes the properties of a system in thermal equilibrium. PIMC is a very efficient method to study dense plasmas [7, 8, 9, 10, 11, 12, 13, 14, 15] where electrons are partially excited because of the high temperature.

Many applications of the PIMC method require an accurate treatment of Coulomb interactions in periodic boundary conditions (PBC). This includes all electronic structure simulations that describe electrons as individual particles. However, there is still no universally accepted method to compute the Coulomb propagator in PBC, which has led to unnecessary approximations resulting in less efficient and less accurate many-body simulations.

In this article, we describe an accurate approach to compute the Coulomb pair density matrix in a periodic system. It can easily be generalized to other long range interactions [16]. The density matrix of a bosonic (B) or fermionic (F) system at temperature T can be expressed in terms of an imaginary-time path integral,

$$\rho_{\rm B/F}(\mathbf{R},\mathbf{R}';\beta) = \frac{1}{N!}\sum_{\mathcal{P}}(\pm 1)^{\mathcal{P}}\int_{\mathbf{R}\to\mathcal{P}\mathbf{R}'} d\mathbf{R}_i\,\rho(\mathbf{R},\mathbf{R}_1;\tau)\,\rho(\mathbf{R}_1,\mathbf{R}_2;\tau)\ldots\rho(\mathbf{R}_{M-1},\mathcal{P}\mathbf{R}';\tau)\;, \tag{1}$$

where τ is the time step $\tau = \beta/M$ with $\beta = 1/k_{\rm B}T$, and $k_{\rm B}$ is Boltzmann's constant. N particles in real-space representation, $\mathbf{R} = \{\mathbf{r}_1,\ldots,\mathbf{r}_N\}$, are described in the canonical ensemble. The sum over $\mathcal{P}$ presents all possible permutations of identical particles. In the fermionic case, odd permutations enter with a negative weight. Atomic units of Bohr radii and Hartree will be used throughout this work.

Instead of employing the propagator at temperature, T, path integrals rely on a density matrix at much higher temperature, $M\times T$. At high temperature, the many-body density matrix can be computed with good accuracy because

Email address: militzer@berkeley.edu (B. Militzer)

exchange effects as well as three-body correlations are negligible in this limit. A novel method of constructing the high temperature density matrix (HTDM) for systems with *long-range interactions* with *periodic boundary conditions* is the focus of this study.

Different approximations for the Coulomb HTDM have been advanced that all become exact in the limit of $\tau \to 0$. However, all PIMC simulations are performed at finite τ. Therefore an accurate representation of the HTDM is very important since its accuracy determines the maximum time step τ one can use. A larger time step allows one to significantly cut down on the number of time slices, M, in the path integral and therefore to improve the efficiency of many-body simulations. Such a efficiency gain may be crucial in practical applications in order to perform accurate simulations at low temperature or of large systems.

The HTDM can be used to define the potential action, $U(\mathbf{R}, \mathbf{R}'; \tau)$. For a system of N distinguishable particles in real space representation this reads,

$$\rho(\mathbf{R}, \mathbf{R}'; \tau) = \exp\{-U(\mathbf{R}, \mathbf{R}'; \tau)\} \prod_{i=1}^{N} \rho_0(\mathbf{r}_i, \mathbf{r}_i'; \tau) \quad . \tag{2}$$

ρ_0 is the free particle density matrix in D dimensions,

$$\rho_0(\mathbf{r}, \mathbf{r}'; \tau) = (4\pi\lambda\tau)^{-D/2} \exp\{-(\mathbf{r} - \mathbf{r}')^2/4\lambda\tau\} \quad . \tag{3}$$

λ is the a mass dependent parameter, $\hbar^2/2m$. U is commonly approximated as the product over the nonideal parts of all pair density matrices $\rho(\mathbf{r}_{ij}, \mathbf{r}'_{ij}; \tau)$,

$$\exp\{-U(\mathbf{R}, \mathbf{R}'; \tau)\} \approx \exp\left\{-\sum_{i<j} u(\mathbf{r}_{ij}, \mathbf{r}'_{ij}; \tau)\right\} = \prod_{i<j} \frac{\rho(\mathbf{r}_{ij}, \mathbf{r}'_{ij}; \tau)}{\rho_0(\mathbf{r}_{ij}, \mathbf{r}'_{ij}; \tau)} \quad . \tag{4}$$

This is called the *pair approximation*, and is accurate to order τ^2 [4, 5, 6]. One essentially starts with a exact solution of the two-body problem when performing many-body simulations. This means only one time slice is needed to simulate the hydrogen atom at any temperature but more slices are needed for the hydrogen molecule because in this case, three-body correlations are important. Exchange effects have been neglected in Eq. 4, which is well justified for small time steps, τ. In the full path integral, Eq. 1, are included however because of the sum over permutations.

For a Coulomb system with periodic boundary conditions, these pair density matrices, $\rho(\mathbf{r}, \mathbf{r}'; \tau)$, are solutions of the two particle Bloch equation with the Ewald potential [17],

$$\frac{\partial \rho}{\partial \tau} \; = \; -\hat{H}\rho \; = \; \lambda_{ij} \nabla^2_{\mathbf{r}} \rho \; - \; V_{\mathrm{EW}}(\mathbf{r})\rho \; , \tag{5}$$

with the initial condition $\rho(\mathbf{r}, \mathbf{r}'; \tau = 0) = \delta(\mathbf{r} - \mathbf{r}')$. The reduced mass $\mu_{ij} = m_i m_j/(m_i + m_j)$ enters through $\lambda_{ij} \equiv \hbar^2/2\mu_{ij}$. The pair density matrix can also be derived from the Feynman-Kac relation,

$$\rho(\mathbf{r}, \mathbf{r}'; \tau) = \rho_0(\mathbf{r}, \mathbf{r}'; \tau) \; \left\langle e^{-\int_0^\beta dt \, V(\mathbf{r}(t))} \right\rangle_{\mathbf{r} \to \mathbf{r}'} \quad , \tag{6}$$

where the average is to be taken over all free-particle (Brownian) paths from $\mathbf{r}$ to $\mathbf{r}'$. For potentials without negative singularities, this expression can easily be evaluated numerically for specific pairs of $\mathbf{r}$ and $\mathbf{r}'$, which enables one to verify the approximations in the computation of the pair density matrix that we will introduce below. However, the results of Feynman-Kac calculations always have a statistical uncertainty due to the finite sample of Brownian paths.

The resulting Ewald pair action, $u_{\mathrm{EW}}(\mathbf{r}, \mathbf{r}'; \tau) = -\ln[\rho_{\mathrm{EW}}/\rho_0)]$, determines the weight of the paths in Eq. 1 where $\mathbf{r}$ and $\mathbf{r}'$ represent the separations of pairs of particles i and j at two adjacent time slices at t and $t + \tau$,

$$\mathbf{r} = \mathbf{r}_i(t) - \mathbf{r}_j(t) \quad , \quad \mathbf{r}' = \mathbf{r}_i(t + \tau) - \mathbf{r}_j(t + \tau) \quad . \tag{7}$$

For a spherically symmetric potential, the pair density matrix depends on τ and three spatial variables: the initial and final pair separations $|\mathbf{r}|$ and $|\mathbf{r}'|$ as well as the angle between them θ. Alternatively, it can be expressed in terms of the variables q, s and z,

$$q \equiv \frac{1}{2}(|\mathbf{r}| + |\mathbf{r}'|) \; , \; s \equiv |\mathbf{r} - \mathbf{r}'| \; , \; z \equiv |\mathbf{r}| - |\mathbf{r}'|. \tag{8}$$

For the Coulomb potential, the dependence on z drops out [18]. The Ewald potential, however, has the symmetry of the periodic simulation cell which requires both the initial and final pair separation to be specified with respect to the cell. This implies that the pair density matrix for the Ewald potential depends on six spatial variables. This makes computation and storage of the corresponding action extremely awkward.

Previous methods [19, 20] to deal with this difficulty have involved a break-up of the Ewald potential into a spherically symmetric short-range piece and a long-range remainder,

$$V_{\mathrm{EW}}(\mathbf{r}) = V_{\mathrm{s.r.}}(|\mathbf{r}|) + V_{\mathrm{l.r.}}(\mathbf{r}) \; . \tag{9}$$

The short-range piece has been treated numerically using the matrix squaring technique developed by Storer [21]. In principle, it allows one to derive the exact action for a spherically symmetric potential but in practice the accuracy is controlled by numerical accuracy of the integration. Matrix squaring is performed on a grid and controlling the associated grid errors requires significant care [22]. To treat the cusp condition at the origin accurately, the short-range part must include the singular part of the potential. Most simply, one can use the direct $1/r$ interaction term as short-range part. Alternatively, one can employ the optimized Ewald break-up method described in [23, 24], which allows one to construct a short-range piece that always decays within the boundaries of the simulation cell. A detailed review of the break-up method and its accuracy is given in [22]. The *primitive approximation*,

$$u_{\mathrm{P.A.}}(\mathbf{r}, \mathbf{r}'; \tau) = \frac{\tau}{2} \left[V(\mathbf{r}) + V(\mathbf{r}') \right] \; , \tag{10}$$

provides a simple straightforward way to add the long-range remainder,

$$u(\mathbf{r}, \mathbf{r}'; \tau) \approx u_{\mathrm{s.r.}}(\mathbf{r}, \mathbf{r}'; \tau) + \frac{\tau}{2} \left[V_{\mathrm{l.r.}}(\mathbf{r}) + V_{\mathrm{l.r.}}(\mathbf{r}') \right] \; . \tag{11}$$

but the random phase approximation has also been applied to the long-range action [20]. When we later refer to Eqs. 9 and 11, we assume that the $1/r$ potential has been used as short-range piece.

The break-up of the Ewald potential [19, 20] introduces an additional approximation to path integral computation. While it has been successfully in many applications [25, 26, 27, 28] there is a need for improvement. The break-up is *ad hoc* and introduces some arbitrariness to the construction of the Ewald action. The accuracy remains high if either potential piece is sufficiently smooth on the scale of the thermal de Broglie wave length, $\lambda_d = \sqrt{4\pi\lambda\tau}$. However, the convergence to the correct answer as function of cell size and temperature is difficult to assess. For these reasons, we present a method here that consistently treats the direct Coulomb interaction within the simulation cell and that with periodic images with the same level of accuracy. Our method thereby avoids introducing a short and long-range potential. The necessary pair density matrices are derived for the Coulomb potential, which makes it possible to utilize the large amount of analytic and numerical work available for this potential. The development of the method proceeds in steps that we will now described.

2. Method

2.1. Computation of the pair density matrix for the Coulomb potential

It is first necessary to compute the pair density matrix for an isolated pair of particles. This can either be done with matrix squaring or from the sum over eigenstates. In the matrix squaring technique, one can take advantage of the fact that only s-wave contributions enter in case of the Coulomb potential as done by Storer [21]. When using the squaring technique, one starts from a high temperature expansion and then numerically derives the density matrix at successively lower temperatures by performing the following integration numerically,

$$\rho(\mathbf{r}, \mathbf{r}'; 2\tau) = \int \mathbf{dr}'' \, \rho(\mathbf{r}, \mathbf{r}''; \tau) \, \rho(\mathbf{r}'', \mathbf{r}'; \tau) \; , \tag{12}$$

until the lowest temperature of interest has been reached. This typically requires 10–30 iterations. Since the matrix squaring is done on a grid in $\mathbf{r}$ and $\mathbf{r}'$, a grid error is introduced. For the Coulomb potential, this usually requires a high number grid points near the singularity at the origin. This singularity also requires care when the density matrix is

initialized using a high temperature expansion at the beginning of the squaring procedure. Despite these shortcomings, the squaring technique has the advantage that it can easily be applied to arbitrary spherical potentials [29]. Schmidt and Lee developed an alternative approach where kinetic and potential operators are applied repeatedly using Fourier transforms [30]. This method has been adopted by J. Shumway to study a variety of systems with PIMC [31]. Vieillefosse used an analytic power-series expansion method to construct the action [32].

For potentials that do not exhibit negative singularities, the pair density matrix can also be derived from the Feynman-Kac formula, Eq. 6. This approach was applied to the Yukawa interaction in Ref. [16]. It avoids introducing grid errors and readily yields diagonal matrix elements as well as the first term in an expansion for off-diagonal elements but the method is impractical for constructing tables with arbitrary off-diagonal elements. Matrix squaring would be more appropriate [22].

In this paper, we rely on another approach to compute the pair density matrix that relies on the summation of eigenstates [33],

$$\rho(\mathbf{r}, \mathbf{r}'; \tau) = \sum_s e^{-\tau\epsilon_s} \psi_s(\mathbf{r}) \psi_s^*(\mathbf{r}') \; . \tag{13}$$

It also avoids grid errors and can provide off-diagonal elements efficiently. It requires that the eigenstates are known with high precision, which is the case for the Coulomb potential. Although the number of states to be considered increases with temperature, the summation can be performed accurately for the temperature range of interest as was shown in Ref. [33].

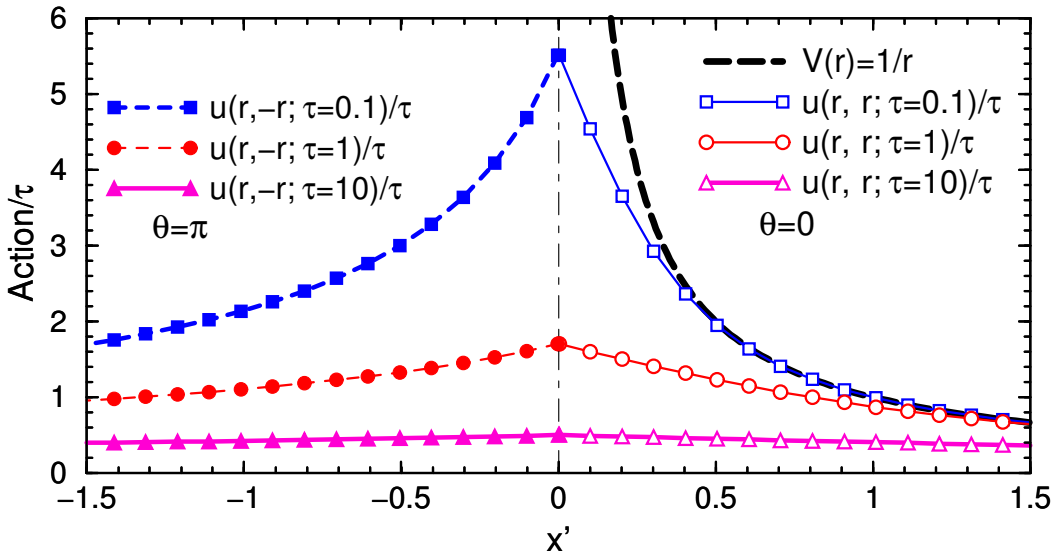

Figure 1: Potential action divided by the inverse temperature τ at $\tau = 0.1, 1.0, 10.0$ for an isolated pair of electrons as a function of x' with $\mathbf{r} = (|x'|, 0, 0)$ and $\mathbf{r}' = (x', 0, 0)$. With increasing separation, the diagonal action ($\mathbf{r} = \mathbf{r}'$) converges rapidly to the primitive action, τ/r. The action in exchange case ($\mathbf{r} = -\mathbf{r}'$) is consistently higher than the diagonal action, $u(\mathbf{r}, -\mathbf{r}, \tau) \geq u(\mathbf{r}, \mathbf{r}, \tau)$.

For illustration, Fig. 1 shows examples of the electron pair potential action for the on diagonal case ($\mathbf{r}' = \mathbf{r}$) and the exchange case ($\mathbf{r}' = -\mathbf{r}$) over two decades of τ. The cusp condition leads to a linear behavior near the origin. For large r, the diagonal action converges to the primitive action. The action in the exchange case is always higher than that of the diagonal case, which can be understood from the Feynman-Kac formula in Eq. 6 where one takes an averages over all Brownian paths. In the exchange case, paths beginning at $\mathbf{r}$ must diffuse around the most repulsive part of $1/r$ potential to reach the end point of $-\mathbf{r}$. In the diagonal case, the paths start and end at $\mathbf{r}$ and can therefore better avoid regions of high potential energy near the origin.

To increase the efficiency of PIMC simulations, the HTDM is derived beforehand and tabulated. For a given time step τ, the Coulomb pair action, $u(q, s) \equiv u(\mathbf{r}, \mathbf{r}'; \tau)$, is a function of the two variable q and s, which we have defined in Eq. 8. In order to reduce the storage, we fit the off-diagonal terms using an expansion of powers of s^2 (compare

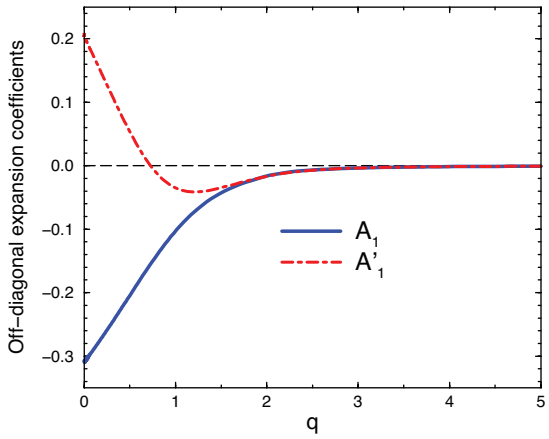

Figure 2: Off-diagonal expansion coefficients for proton-electron pair action A_1 and its τ derivative A_1' at $\tau = 1$. A_1 is defined in Eq. 14.

with [6]),

$$u(q, s) \approx u(q, 0) + \sum_{i=1}^{n} A_i(q)\, s^{2i}, \tag{14}$$

For each q, a least squares fit can represent the off-diagonal term with sufficient accuracy. The results for $n = 1$ are shown in Fig. 2. The expansion works well in PIMC because the kinetic energy prevents adjacent point on the path to exceed separation much larger than the thermal de Broglie wave length for the corresponding τ. The storage of complete set of off-diagonal terms is therefore not needed.

For the Coulomb potential, the off-diagonal action terms decay approximately as $q^{-3.1}$, which means they may be neglected for pair of particles that are far apart and more importantly, contributions from particle images in neighboring periodic simulation cells are typically very small. The decay can be inferred from the slopes of three curves in Fig. 3b. The first compares the diagonal ($s = 0$) and off-diagonal action ($|r| = |r'| = q$, $s = 2\sqrt{\lambda\tau} = \sqrt{2}$) at constant q. The magnitude of s represents a typical separation of adjacent points along the path which is mostly determined by the free particle action. The second curve in Fig. 3b shows the error in the primitive approximation for the same q and s parameters. The third curve shows the error in the primitive approximation for parallel vectors ($\theta = 0$) with the exact action. The graph shows that, for large separations, the primitive approximation works well and off-diagonal contributions may be neglected. Since the difference between diagonal and off-diagonal terms decays faster than q^{-3}, the summation over all periodic images converges.

These properties are taken advantage of in PIMC simulations, where one typically computes the off-diagonal contributions only for particle pairs within the simulation cell using the minimum imagine convention. To date, no efficient way has been proposed to sum up all off-diagonal contributions. However, if necessary, a summation over the required number of images can be included easily in PIMC simulations.

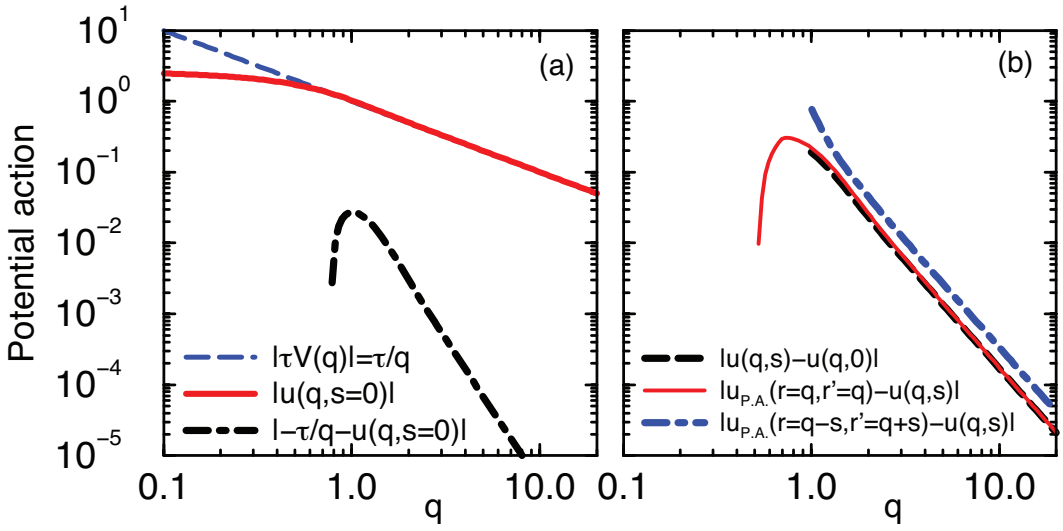

Figure 3: The potential pair action, $u(q, s)$, for a proton-electron pair ($\tau = 1$, $\lambda = 1/2$) shown as function of $q = \frac{1}{2}[|\mathbf{r}| + |\mathbf{r}'|]$. The left and right panels compare the magnitude of the error in the primitive approximation for different diagonal and off-diagonal action terms, respectively. The left graphs shows that, for diagonal configurations, $q = \mathbf{r} = \mathbf{r}'$ and $s = 0$, the deviation between the primitive approximation, $-\tau/q$, and the exact action, $u(q, s = 0)$, decays like $q^{-4.1}$. Since the interaction is attractive, the potential and the action are negative. Near the cusp, one finds $u > \tau V$ while for large q, one find $u < \tau V$ instead. Since we use a log scale and are interested in the large q limit, we omitted curve sections for small q where the action difference has opposite sign. The right graphs shows that the off-diagonal terms decays like $q^{-3.1}$ for fixed $s = |\mathbf{r} - \mathbf{r}'| = 2\sqrt{\lambda\tau} = \sqrt{2}$ (dashed line). The dot-dashed line shows the error in the primitive approximation for parallel $\mathbf{r}$ and $\mathbf{r}'$ ($\theta = 0$). The solid line shows this error in the case of $|\mathbf{r}| = |\mathbf{r}'|$ and angle $\theta > 0$.

2.2. *Pair approximation for the image charges*

The pair approximation Eq. 4 is commonly used to approximate the action of a path. This expression follows from the Feynman-Kac formula Eq. 6, here written for a *finite* system of N particles,

$$\exp\{-U(\mathbf{R},\mathbf{R}';\tau)\} = \left\langle \exp\left\{-\int_0^\tau dt \sum_{i<j}^{N} \frac{Q_i Q_j}{|\mathbf{r}_{ij}(t)|}\right\}\right\rangle_{\mathbf{R}\to\mathbf{R}'} \tag{15}$$

$$= \left\langle \prod_{i<j}^{N} \exp\left\{-\int_0^\tau dt\, \frac{Q_i Q_j}{|\mathbf{r}_{ij}(t)|}\right\}\right\rangle_{\mathbf{R}\to\mathbf{R}'} \tag{16}$$

$$\approx \prod_{i<j} \left\langle \exp\left\{-\int_0^\tau dt\, \frac{Q_i Q_j}{|\mathbf{r}_{ij}(t)|}\right\}\right\rangle_{\mathbf{r}_{ij}\to\mathbf{r}'_{ij}} \tag{17}$$

$$= \prod_{i<j} \exp\left\{-u(\mathbf{r}_{ij},\mathbf{r}'_{ij};\tau)\right\} \tag{18}$$

$$= \exp\left\{-\sum_{i<j} u(\mathbf{r}_{ij},\mathbf{r}'_{ij};\tau)\right\} \tag{19}$$

The pair approximation enters in Eq. 17 where it is assumed that interactions between pairs of particles may be averaged independently from the location of paths of the remaining particles. This approximation becomes increasingly accurate for large separations. It is exact at high temperature and, as stated before, the error is of $O(\tau^3)$.

Now we will describe how the pair approximation can be applied to the systems with periodic boundary conditions. In principle, one only has to add sum over the interaction with of all periodic images using the pair approximation, which assumes that the diffusion of paths of the image particles may also be averaged independently. Since the error in the pair approximation also decreases with separation, applying it to the periodic images in neighboring cells is less of an approximation than the pair approximation to the interaction of particle pairs within the simulation cell.

However, Eq. 19 converges only *conditionally* since the Coulomb potential is long-ranged. This problem has been solved by introducing the Ewald potential which assumes charge neutrality by introducing a neutralizing background. Starting from the Ewald potential, we will now give an approximate expression for the corresponding Ewald action. Since the exact action converges to the primitive approximation for large separations (Fig. 3a), the correction to the primitive action is a short-ranged function,

$$\Delta u(\mathbf{r},\mathbf{r}';\tau) = u(\mathbf{r},\mathbf{r}';\tau) - \frac{\tau}{2} Q_i Q_j \left(\frac{1}{|\mathbf{r}|} + \frac{1}{|\mathbf{r}'|} \right) . \tag{20}$$

Since it decays faster than r^{-3} (Fig. 3a), the sum over all images converges. This allows us to construct an Ewald action using the primitive approximation and a sum of corrections Δu,

$$u_{\mathrm{EW}}(\mathbf{r},\mathbf{r}';\tau) \approx \frac{\tau}{2} Q_i Q_j [V_{\mathrm{EW}}(\mathbf{r}) + V_{\mathrm{EW}}(\mathbf{r}')] + \sum_{\mathbf{L}} \Delta u(\mathbf{r}+\mathbf{L},\mathbf{r}'+\mathbf{L};\tau) + u_{\mathrm{BG}} \quad , \tag{21}$$

which is the central result of this article. It should be noted that $u(\mathbf{r},\mathbf{r}';\tau)$ does not need to go to zero within the simulation cell, while the short-range term in Eq. 9 does.

We note that the expression in Eq. 21 is periodic in space, symmetric in the arguments $\mathbf{r}$ and $\mathbf{r}'$, and satisfies the cusp condition, i.e. the $1/r$ singularity in the Coulomb potential as $r \to 0$ is canceled in the Bloch equation by a term arising from the kinetic energy operator.

The background term u_{BG} in Eq. 21 requires further discussion. The need to introduce this term the can be demonstrated in two ways. First, one can analyze the residual of Bloch equation,

$$R(\mathbf{r},\mathbf{r}';\tau) \equiv \frac{1}{\rho(\mathbf{r},\mathbf{r}';\tau)} \left[\frac{\partial}{\partial \tau} - \lambda_{ij} \nabla^2_{\mathbf{r}} + V \right] \rho(\mathbf{r},\mathbf{r}';\tau) . \tag{22}$$

For the diagonal matrix elements, the residual derived from the primitive action leads to the following simple expression,

$$R(\mathbf{r},\mathbf{r};\tau) = \frac{\lambda\tau}{2} \nabla^2_{\mathbf{r}} V - \frac{\lambda\tau^2}{4} (\nabla_{\mathbf{r}} V)^2 \quad . \tag{23}$$

For the Ewald potential, the presence of a neutralizing charge background gives rise a constant, $\mathbf{r}$ independent term, $\nabla^2_{\mathbf{r}} V_{\mathrm{EW}} = 4\pi/\Omega$, where Ω is the volume of the simulation cell. The second term in Eq. 23 is small and only weakly $\mathbf{r}$-dependent. We chose to approximate it by assuming a locally harmonic potential [3] at the point $\mathbf{r}^* = (L/2, L/2, L/2)$,

$$u_{\mathrm{BG}} = \frac{2}{3} Q_i Q_j \frac{\pi\lambda\tau^2}{\Omega} - \sum_{\mathbf{L}} \Delta u(\mathbf{r}^*+\mathbf{L},\mathbf{r}^*+\mathbf{L};\tau) \quad . \tag{24}$$

The first term is of order $O(\tau^2)$ and is therefore not included in the primitive approximation. One could argue that the u_{BG} term is not important because it is a constant and, in PIMC simulations, only the relative weight between different paths matters for the configuration sampling. However, the kinetic energy is derived from the τ derivative of the action [6] and therefore u_{BG} introduces a small correction.

The second way to derive the background term is by numerical calculations using the Feynman-Kac formula given in Eq. 6. In Fig. 4, the difference of the various approximations for the Ewald action are compared with the computed exact values. The graphs shows that the error in the primitive approximation approaches a constant at large r while it decays to zero for a pair of isolated particles. The difference primarily arises from the presence of the neutralizing background, which was corrected by introducing u_{BG}. However, it should be stressed that, $\tau = 1$ in Fig. 4 is much larger than typical time steps used in simulations with electrons and nuclei. In practical simulations, the background term is less important because it scales like τ^2.

In analogy to Ewald approach (Eq. 29), the action of a many-body system can be written as,

$$U(\mathbf{R},\mathbf{R}';\tau) = \sum_{i>j} u_{\mathrm{EW}\,ij}(\mathbf{r}_{ij},\mathbf{r}'_{ij};\tau) + \sum_i \tau\, Q_i^2 V_{\mathrm{M}} . \tag{25}$$

where the charge factors have been included in the action terms. The efficient evaluation of u_{EW} is discussed in Appendix A. V_{M} is defined in Eq. 30.

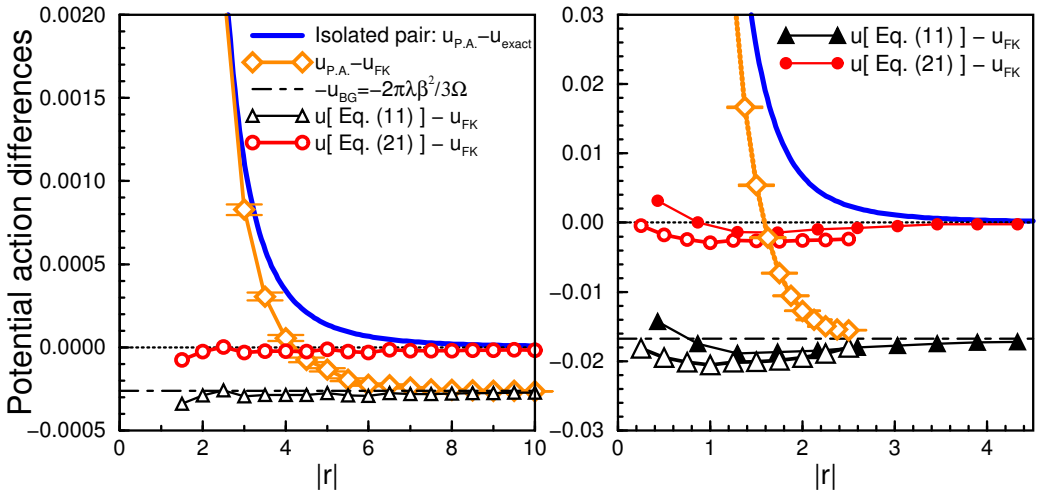

Figure 4: Various approximations for the Ewald action for pair of electrons at $\tau = 1$ are compared on the diagonal as a function of $|\mathbf{r}|$ with the exact action u, which was either computed from the sum over eigenstates (Eq. 13) or using the Feynman-Kac formula (Eq. 6). The left graph shows action difference along the (1,0,0) direction in a cubic cell of 20 a.u. size. The right graph repeats all those curves with open symbols for a smaller cell of 5 a.u. but results for the (1,1,1) direction have been added with filled symbols. The error in the primitive approximation $u_{\mathrm{P.A.}}$ does not decay to zero, underlining contributions of the neutralizing charge background (dot-dashed line).

In summary we now reiterate the steps in our preferred method to compute the HTDM in periodic boundary conditions. First we use the sum over Coulomb eigenstates, Eq. 13 to compute diagonal and off-diagonal elements. The off-diagonal elements are expanded in power of s using Eq. 14 and then tabulated. In PIMC simulations, we typically evaluate them only for pairs of particles in the simulation cell using the minimum image convention. Because the diagonal matrix elements decay more slowly, we apply the optimized Ewald break-up method, Eq. 35, to evaluate them efficiently during PIMC computations. Diagonal and off-diagonal elements are then combined to evaluate the total action in Eq. 25.

3. Results

Tables 1 and 2 give the density matrices and their τ derivative for isolated proton-electron and electron-electron pairs at a time step of 0.125 Hartrees^{-1}, which is typical for a PIMC simulation. In the notation of Eq. 14, the diagonal and first order off-diagonal expansion coefficients are tabulated.

To reach a high precision with PIMC computations, one needs to treat the interactions accurately at all length scales. Before we test the accuracy of our HTDM in periodic boundary conditions, we analyze the accuracy of PIMC simulations of the hydrogen atom and molecule in order to probe the accuracy of our diagonal and off-diagonal short-range action.

First we performed PIMC simulations of a single hydrogen atom at a temperature $T = 0.025$. This temperature was chosen low enough for the atom to be in the ground state since the relative occupation probability of the first excited state is 5×10^{-5}. Path integral Monte Carlo estimates of the potential energy agrees with the exact value of -1 within the statistical error bar of the Monte Carlo integration, here 10^{-4}. While the evaluation of the potential energy involves only the action, the total energy estimator requires also the τ derivative. The computed total energy agreed with the exact value of $-1/2$ to a relative accuracy of 7×10^{-4}. Both potential and kinetic energy estimators are necessary to calculate the pressure, P, from the virial theorem, $3\langle P\rangle\Omega = 2\langle K\rangle + \langle V\rangle$.

As a second test for the accuracy of the computed pair density matrix, the kinetic and potential energy for an isolated hydrogen molecule was computed as a function of proton separation R. Fig. 5 shows very good agreement with the exact groundstate calculation [34]. The molecular binding energy of 1.174448 as well as the location of the minimum at $R = 1.4008$ are well reproduced (see inset of figure 5). The virial theorem for a diatomic molecule [34, 35]

Table 1: Density matrix at $\tau^{-1} = 8$ for an isolated proton-electron pair. The columns correspond to diagonal potential action, the first off-diagonal expansion coefficient (see Eq. 14 with $n = 1$), the diagonal τ derivative, and its first expansion coefficient.

r	$u(r,0)$	$A(r)$	$u'(r,0)$	$A'(r)$
0.0	–9.052629e–01	–1.0656e+00	–3.701269e+00	4.6908e+00
0.1	–7.094574e–01	–7.8668e–01	–3.664297e+00	2.2366e+00
0.2	–5.375241e–01	–5.4357e–01	–3.435818e+00	4.3544e–01
0.3	–4.052122e–01	–3.5276e–01	–2.988023e+00	–5.3328e–01
0.4	–3.130127e–01	–2.1872e–01	–2.468529e+00	–8.1126e–01
0.5	–2.512131e–01	–1.3263e–01	–2.019987e+00	–7.2479e–01
0.6	–2.090487e–01	–8.0229e–02	–1.683282e+00	–5.3529e–01
0.7	–1.789567e–01	–4.6185e–02	–1.438155e+00	–3.5572e–01
0.8	–1.564692e–01	–2.7139e–02	–1.255464e+00	–2.1970e–01
0.9	–1.390225e–01	–1.7645e–02	–1.114415e+00	–1.4285e–01
1.0	–1.250863e–01	–1.2256e–02	–1.002118e+00	–9.8852e–02
1.1	–1.136946e–01	–8.9124e–03	–9.105148e–01	–7.1705e–02
1.2	–1.042075e–01	–6.7064e–03	–8.343272e–01	–5.3873e–02
1.3	–9.618330e–02	–5.1838e–03	–7.699461e–01	–4.1601e–02
1.4	–8.930751e–02	–4.0954e–03	–7.148140e–01	–3.2843e–02
1.5	–8.334981e–02	–3.2949e–03	–6.670655e–01	–2.6411e–02
1.6	–7.813769e–02	–2.6922e–03	–6.253068e–01	–2.1571e–02
1.7	–7.353934e–02	–2.2291e–03	–5.884752e–01	–1.7856e–02
1.8	–6.945233e–02	–1.8672e–03	–5.557459e–01	–1.4954e–02
1.9	–6.579581e–02	–1.5801e–03	–5.264687e–01	–1.2653e–02
2.0	–6.250516e–02	–1.3493e–03	–5.001243e–01	–1.0803e–02
2.1	–5.952805e–02	–1.1616e–03	–4.762926e–01	–9.2992e–03
2.2	–5.682170e–02	–1.0073e–03	–4.546301e–01	–8.0633e–03
2.3	–5.435076e–02	–8.7928e–04	–4.348534e–01	–7.0381e–03
2.4	–5.208581e–02	–7.7215e–04	–4.167263e–01	–6.1803e–03
2.5	–5.000210e–02	–6.8181e–04	–4.000506e–01	–5.4569e–03
2.6	–4.807872e–02	–6.0507e–04	–3.846586e–01	–4.8426e–03
2.7	–4.629784e–02	–5.3947e–04	–3.704075e–01	–4.3174e–03
2.8	–4.464419e–02	–4.8304e–04	–3.571749e–01	–3.8657e–03
2.9	–4.310460e–02	–4.3425e–04	–3.448554e–01	–3.4752e–03
3.0	–4.166768e–02	–3.9181e–04	–3.333576e–01	–3.1355e–03

Table 2: Pair density matrix for $\tau^{-1} = 8$ for isolated pair of electrons in the format of Tab. 1.

r	$u(r,0)$	$A(r)$	$u'(r,0)$	$A'(r)$
0.0	6.176418e–01	4.4659e–01	2.435490e+00	–1.6593e+00
0.1	5.191880e–01	3.3730e–01	2.424522e+00	–9.0614e–01
0.2	4.290318e–01	2.4933e–01	2.358555e+00	–3.6651e–01
0.3	3.522642e–01	1.8106e–01	2.218501e+00	–2.2177e–02
0.4	2.903868e–01	1.2962e–01	2.021059e+00	1.6609e–01
0.5	2.422795e–01	9.1878e–02	1.799564e+00	2.4375e–01
0.6	2.055164e–01	6.4773e–02	1.584616e+00	2.5324e–01
0.7	1.774303e–01	4.5605e–02	1.394356e+00	2.2765e–01
0.8	1.557096e–01	3.2174e–02	1.234499e+00	1.8896e–01
0.9	1.385903e–01	2.2809e–02	1.103098e+00	1.4953e–01
1.0	1.248157e–01	1.5221e–02	9.952834e–01	1.1214e–01
1.1	1.135143e–01	1.0485e–02	9.060434e–01	8.1349e–02
1.2	1.040821e–01	7.6096e–03	8.312447e–01	6.0020e–02
1.3	9.609319e–02	5.7381e–03	7.677422e–01	4.5517e–02
1.4	8.924103e–02	4.4539e–03	7.131934e–01	3.5419e–02
1.5	8.329967e–02	3.5366e–03	6.658461e–01	2.8165e–02
1.6	7.809915e–02	2.8606e–03	6.243711e–01	2.2803e–02
1.7	7.350923e–02	2.3497e–03	5.877450e–01	1.8744e–02
1.8	6.942845e–02	1.9556e–03	5.551675e–01	1.5608e–02
1.9	6.577663e–02	1.6462e–03	5.260046e–01	1.3144e–02
2.0	6.248957e–02	1.3996e–03	4.997475e–01	1.1178e–02
2.1	5.951525e–02	1.2005e–03	4.759834e–01	9.5902e–03
2.2	5.681109e–02	1.0377e–03	4.543740e–01	8.2918e–03
2.3	5.434190e–02	9.0340e–04	4.346395e–01	7.2197e–03
2.4	5.207834e–02	7.9148e–04	4.165462e–01	6.3261e–03
2.5	4.999577e–02	6.9745e–04	3.998978e–01	5.5751e–03
2.6	4.807331e–02	6.1784e–04	3.845282e–01	4.9393e–03
2.7	4.629319e–02	5.4998e–04	3.702955e–01	4.3971e–03
2.8	4.464018e–02	4.9176e–04	3.570782e–01	3.9319e–03
2.9	4.310111e–02	4.4153e–04	3.447714e–01	3.5305e–03
3.0	4.166463e–02	3.9794e–04	3.332844e–01	3.1821e–03

reads,

$$2K + V = -R\,\frac{dE}{dR}\ . \tag{26}$$

It goes to zero at the equilibrium bond length as well as in the limit of $R \to \infty$ as shown in Fig. 5.

A more detailed analysis of the comparison with the groundstate calculation for R fixed at the equilibrium bond length shown in Fig. 6 reveals that the finite time step in the path integral determines the accuracy of the calculation. The temperature $T = 0.025$ was chosen low enough to compare with the groundstate result as the check with $T = 0.0125$ shows. The internal energy converges faster to the exact groundstate result than the virial term $2K + V$. For $\tau \leq 0.25$, we find that the energy deviates less than 10^{-3} from the exact groundstate energy. For $\tau = 0.0625$, the energy deviated by $(2.4 \pm 1.7) \times 10^{-4}$. For this time step, we obtained $2K + V = (9 \pm 7) \times 10^{-4}$, which corresponds to an residual inaccuracy in the pressure equivalent to the pressure of an ideal molecular gas at $T = 90 \pm 70$ K. This is four times more accurate than the tables used in [36, 27] and more than sufficient for the majority of PIMC simulations of hot, dense hydrogen [26, 37]. We attributed the increase in accuracy to using the sum over eigenstates, Eq. 13, instead of the matrix squaring technique, Eq. 12. This concludes the accuracy analysis for isolated systems of particles.

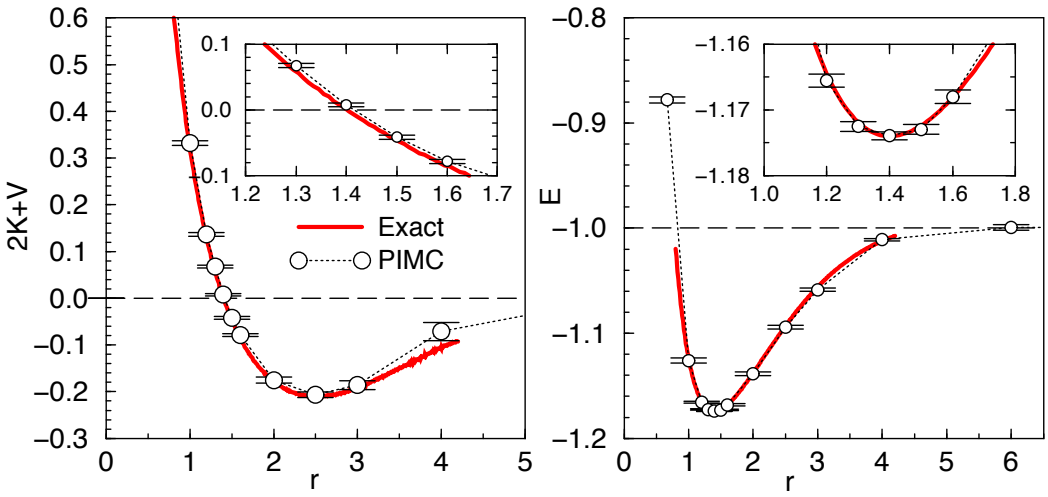

Figure 5: Virial term $2K + V$ (kinetic energy K and potential energy V) and total internal energy E are shown for an isolated hydrogen molecule, for which the nuclei have been kept fixed at separation, r. The PIMC results have been obtained from simulations at $T = 0.0125$ with 320 time slices. The solid lines are the exact groundstate results of [34]. The insets show an enlarged version of the comparison in the region of the equilibrium bond length of r=1.4, which matters most for PIMC simulations of molecular hydrogen.

The accuracy of the constructed pair density matrix in a periodic system is analyzed by calculating the error in Bloch equation 5 for the Ewald potential. The optimized Ewald break-up of Eq. 35 for a cubic simulation cell of size $L = 5$ using 20 k-shells is given in Tables 3 and 4.

Based on the residual in Eq. 22, we define the accuracy parameter,

$$I(L;\tau) = \iint \mathbf{dr}\,\mathbf{dr}'\rho(\mathbf{r},\mathbf{r}';\tau)\left|R(\mathbf{r},\mathbf{r}';\tau)\right| \Big/ \iint \mathbf{dr}\,\mathbf{dr}'\rho(\mathbf{r},\mathbf{r}';\tau)\ , \tag{27}$$

that characterizes the accuracy of the particular approximation to the density matrix. Fig. 7 shows this accuracy parameter for the periodic proton-electron pair density matrix as a function of cell size L. This present method of treating the image charges in the pair approximation is contrasted with treating them in the primitive approximation, Eq. 11, with the long range term $V_{l.r.}(\mathbf{r}) = V_{EW}(\mathbf{r}) - 1/r$. In the limit of large L, both methods are in agreement and show a rapid decay of the residual indicating that the Bloch equation is satisfied with increasing accuracy. In this limit, the residual is dominated by inaccuracies in the offdiagonal elements, which neither method treats exactly. For small L, the pair approximation yields a smaller residual demonstrating that the method proposed here leads to a more accurate high temperature density matrix for periodic systems.

Table 3: Real space part W of the action for proton-electron and electron-electron pair density matrices computed for $\tau^{-1} = 8$ using an optimized Ewald break-up for a cubic simulation cell of size $L = 5$. The k-space part is given in Tab. 4.

r	$W_{\mathrm{pe}}(r)$	$W'_{\mathrm{pe}}(r)$	$W_{\mathrm{ee}}(r)$	$W'_{\mathrm{ee}}(r)$
0.0	–3.948972e–01	–2.462608e+00	3.779454e–01	1.247426e+00
0.1	–2.350750e–01	–2.258029e+00	2.919260e–01	1.196514e+00
0.2	–1.160451e–01	–1.852593e+00	2.190901e–01	1.083259e+00
0.3	–3.789284e–02	–1.376056e+00	1.608496e–01	9.211309e–01
0.4	8.202359e–03	–9.633273e–01	1.163420e–01	7.390493e–01
0.5	3.255803e–02	–6.601111e–01	8.329489e–02	5.647894e–01
0.6	4.338204e–02	–4.511075e–01	5.925357e–02	4.155765e–01
0.7	4.616727e–02	–3.082067e–01	4.188614e–02	2.972913e–01
0.8	4.420917e–02	–2.096609e–01	2.939746e–02	2.081889e–01
0.9	3.948008e–02	–1.413132e–01	2.041829e–02	1.432097e–01
1.0	3.338766e–02	–9.395882e–02	1.400554e–02	9.683606e–02
1.1	2.703458e–02	–6.140030e–02	9.466156e–03	6.429422e–02
1.2	2.110379e–02	–3.929014e–02	6.284010e–03	4.181878e–02
1.3	1.587569e–02	–2.453568e–02	4.085855e–03	2.657455e–02
1.4	1.142789e–02	–1.489252e–02	2.581234e–03	1.644121e–02
1.5	7.866995e–03	–8.749983e–03	1.587436e–03	9.870341e–03
1.6	5.231115e–03	–4.948775e–03	9.427062e–04	5.723989e–03
1.7	3.356079e–03	–2.677517e–03	5.456568e–04	3.186790e–03
1.8	2.013496e–03	–1.378287e–03	3.001534e–04	1.692584e–03
1.9	1.098643e–03	–6.634200e–04	1.574300e–04	8.477546e–04
2.0	5.739410e–04	–2.995616e–04	7.289096e–05	3.991008e–04
2.1	3.066066e–04	–1.223001e–04	2.820100e–05	1.695370e–04
2.2	1.462296e–04	–4.510938e–05	1.383209e–05	6.587290e–05
2.3	3.113736e–05	–1.503693e–05	3.426564e–06	1.986137e–05
2.4	–1.417605e–05	–4.564337e–06	6.935208e–07	6.273595e–06
2.5	0	0	0	0

Table 4: K-space action for proton-electron and electron-electron pair density matrices computed for $\tau^{-1} = 8$ using an optimized Ewald break-up with 20 k-shells for a cubic simulation cell of size $L = 5$. The corresponding real space parts are listed in Tab. 3. The table also includes the Madelung and the background constant from Eqs. 25 and 35.

$n^2, k = 2\pi n/L$	$\tilde{u}_{k,\mathrm{pe}}$	$\tilde{u}'_{k,\mathrm{pe}}$	$\tilde{u}_{k,\mathrm{ee}}$	$\tilde{u}'_{k,\mathrm{ee}}$
u_M	3.5466e–02	2.8372e–01	–3.5467e–02	2.8376e–01
C_u	–3.0502e–03	2.0762e–02	–2.9417e–03	–2.2041e–02
1	–9.8752e–03	–4.5714e–02	5.4742e–03	4.4979e–02
2	–5.0783e–03	–1.6276e–02	1.8624e–03	1.5781e–02
3	–3.1684e–03	–7.6607e–03	8.3439e–04	7.3217e–03
4	–2.0962e–03	–4.0198e–03	4.1473e–04	3.7862e–03
5	–1.4182e–03	–2.2280e–03	2.1645e–04	2.0676e–03
6	–9.6702e–04	–1.2727e–03	1.1557e–04	1.1634e–03
8	–4.4850e–04	–4.3268e–04	3.3300e–05	3.8330e–04
9	–3.0283e–04	–2.5364e–04	1.7587e–05	2.2113e–04
10	–2.0262e–04	–1.4824e–04	9.0566e–06	1.2710e–04
11	–1.3405e–04	–8.5951e–05	4.4823e–06	7.2484e–05
12	–8.7505e–05	–4.9194e–05	2.0841e–06	4.0853e–05
13	–5.6226e–05	–2.7704e–05	8.7102e–07	2.2662e–05
14	–3.5469e–05	–1.5293e–05	2.9069e–07	1.2311e–05
16	–1.3175e–05	–4.2131e–06	–5.3452e–08	3.3414e–06
17	–7.6876e–06	–2.0560e–06	–7.1360e–08	1.6470e–06
18	–4.3189e–06	–9.4808e–07	–6.0744e–08	7.6995e–07
19	–2.3129e–06	–4.0035e–07	–4.2831e–08	3.3463e–07
20	–1.1631e–06	–1.3415e–07	–2.6457e–08	1.3167e–07
21	–5.3551e–07	–1.5653e–08	–1.4397e–08	4.4726e–08
22	–2.1498e–07	1.9113e–08	–6.7088e–09	1.1253e–08

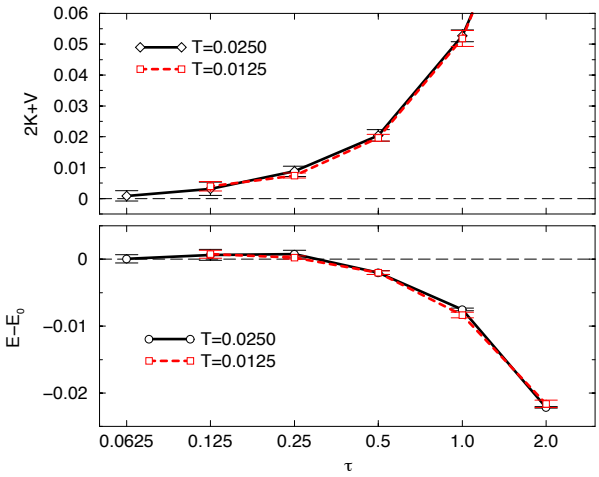

Figure 6: Total internal energy E and virial term $2K + V$ for an isolated hydrogen molecule are shown for different temperatures as a function of the time step in the path integral. The nuclei have been kept fixed at the equilibrium separation of $R = 1.4008$.

We have applied Eq. 21 to PIMC simulations of hydrogen, helium, and heavier elements [38, 39, 40, 41, 42, 43], and to study quantum effects in the one-component plasma [44, 45, 16]. Fig. 8 demonstrates the quality of the construct density matrices in PIMC simulation of a strong coupled Coulomb system. Despite significant quantum properties the particles arrange in a Wigner crystal. The presented time step analysis shows that a time step of 400 or less is needed to obtain converged structural properties such as pair correlation functions. This implies that some simulations in [44] and [45] could have been performed with fewer time slices, which would have reduced the computational cost. Our results as a benchmark for future methods to construct density matrices for PIMC that would then need to demonstrate that the same level of accuracy can be achieved with larger time steps.

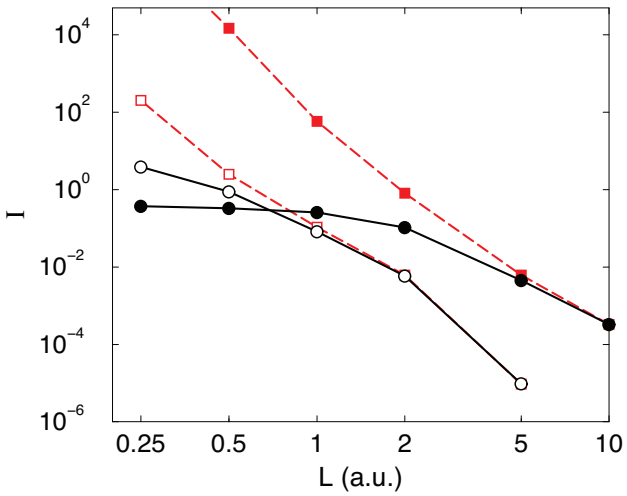

Figure 7: Residual of the Bloch equation $I(L;\tau)$ in periodic boundary conditions is shown as function of cell size L for the proton-electron pair density matrix at two different temperatures (open symbols $\tau^{-1} = 8$ and full symbols $\tau^{-1} = 0.5$). The pair approximation for periodic images (circle) is compared with treating the images in the primitive approximation (squares).

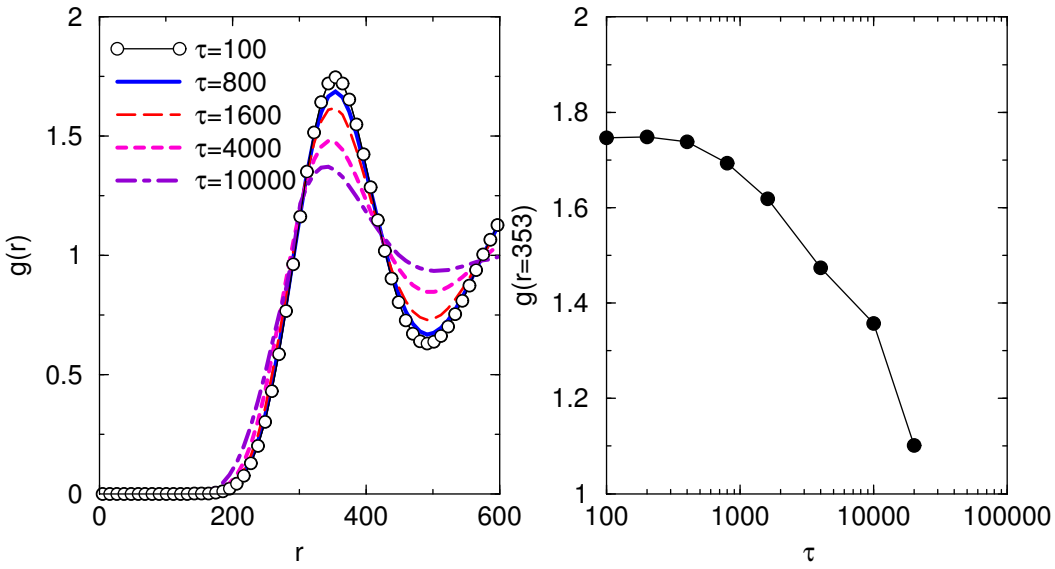

Figure 8: The pair correlation function $g(r)$ for the homogeneous electron gas in state of a Wigner crystal [25, 44, 45, 16] for coupling parameter $\Gamma = 200$ and quantumness parameter $\eta = 1$ ($\beta = 40000, r_s = 200$) are shown from simulation with different time steps τ. The right graph shows how the maximum value of the $g(r)$ converges as a function of τ. Good convergence is reached for $\tau = 400$ requiring simulations with 100 time slices.

4. Conclusions

The method proposed here to compute the Coulomb pair density matrix in periodic boundary conditions has two advantages over previous approaches. It starts from the more accurate Coulomb pair density matrix, which reduces the numerical errors in the short-range behavior of the computed pair density matrix and circumvents a break-up of the potential. Although it does not derive the pair density matrix for the Ewald potential exactly, it consistently uses the pair approximation for the action which is an intrinsic assumption in most many-body path integration simulations.

In addition to describing this method, quantitative test results for the isolated hydrogen atom and molecule as well as a test for the periodic system based on the residual error in the Bloch equation were presented to assess the accuracy of the high temperature density matrix. It is suggested that these tests should form a basis for comparing any proposed alternative methods.

A. Ewald potential

The Ewald method to describe the potential of charged particles in periodic boundary conditions can be adapted in the following way to calculate the action. The potential energy of a system of N charges Q_i interacting via the Coulomb potential $V_c(\mathbf{r}) \equiv 1/|\mathbf{r}|$ is given by [46],

$$V = \sum_{i>j} \sum_{\mathbf{L}} Q_i Q_j \, V_c(\mathbf{r}_{ij} + \mathbf{L}) \; + \; \frac{1}{2} \sum_{\mathbf{L}\neq 0} \sum_{i} Q_i^2 \, V_c(\mathbf{L}) \; . \tag{28}$$

where $\mathbf{r}_{ij} = \mathbf{r}_i - \mathbf{r}_j$ and $\mathbf{L}$ is a lattice vector. This expression converges *conditionally* for charge neutral systems ($\sum_i Q_i = 0$). Under the assumption of charge neutrality, this expression can be computed from Ewald potential, $V_{\rm EW}$,

$$V = \sum_{i>j} Q_i Q_j \, V_{\rm EW}(\mathbf{r}_{ij}) \; + \; \sum_{i} Q_i^2 \, V_{\rm M} \; , \tag{29}$$

and the Madelung constant, $V_{\rm M}$,

$$V_{\rm M} = \frac{1}{2} \lim_{r\to 0} [V_{\rm EW}(r) - V_c(r)] \; . \tag{30}$$

The Ewald potential is split in a real space and a Fourier part [17] by subtracting the screening potential $V_s(r)$ of a Gaussian charge distribution. Under the assumption of charge neutrality ($\sum_i Q_i = 0$) or in the presence of a neutralizing background, the Ewald potential becomes,

$$V_{\mathrm{EW}}(\mathbf{r}) = \sum_{\mathbf{L}} \left[V_c - V_s\right](\mathbf{r}+\mathbf{L}) + \sum_{\mathbf{k}\neq 0} \tilde{V}_s(\mathbf{k}) e^{i\mathbf{k}\cdot\mathbf{r}} + C_V \ , \tag{31}$$

where the constant C_V,

$$C_V = -\frac{1}{\Omega}\int \mathbf{d}^3\mathbf{r}\ \left[V_c - V_s\right](\mathbf{r}) \ , \tag{32}$$

represents contributions from a neutralizing background. For neutral systems, all C_V terms cancel.

The total potential energy can be computed more efficiently by introducing the Fourier transform of the charge density, $\tilde{\rho}(\mathbf{k}) = \sum_j Q_j e^{-i\mathbf{k}\mathbf{r}_j}$. Eq. 28 then reads,

$$V = \sum_{i>j} Q_i Q_j \left[\sum_{\mathbf{L}} \left[V_c - V_s\right](\mathbf{r}+\mathbf{L}) + \frac{1}{2} C_V \left|\tilde{\rho}(0)\right|^2 + \frac{1}{2}\sum_{\mathbf{k}\neq 0} \tilde{V}_s(\mathbf{k}) \left|\tilde{\rho}(\mathbf{k})\right|^2\right] + \sum_i Q_i^2\, V_{\mathrm{image}} \ , \tag{33}$$

where the constant V_{image} has been introduced,

$$2V_{\mathrm{image}} = 2V_{\mathrm{M}} - C_V - \sum_{\mathbf{k}\neq 0} \tilde{V}_s(\mathbf{k}) = \sum_{\mathbf{L}\neq 0} \left[V_c - V_s\right](\mathbf{L}) - V_s[0] \ . \tag{34}$$

In contrast to V_{M}, V_{image} depends on the choice of V_s.

The same approach can be applied to construct the diagonal Ewald action where $V_c(r)$ is then replaced by $\tau V_c(r) + \Delta u(\mathbf{r}, \mathbf{r}; \tau)$. In many-body Monte Carlo simulations, an efficient computation of the Ewald action, Eq. 21, is crucial. This can be achieved by using the optimized Ewald break-up technique developed by Natoli *et al.* [23],

$$u_{\mathrm{EW}}(\mathbf{r}) \approx \sum_n a_n f_n(|\mathbf{r}|) + \sum_{|\mathbf{k}|\leq k_c} y_{|\mathbf{k}|}\, e^{-i\mathbf{k}\cdot\mathbf{r}} + C_u \ . \tag{35}$$

where one uses only one real-space image and a variable number of Fourier vectors depending on the required accuracy. As basis set f_n, we use locally piecewise quintic Hermite interpolants as suggested in [23]. However, this basis set is only used to perform the break-up.

The coefficients a_n and $y_{\mathbf{k}}$ are chosen to minimize the mean squared deviation between the $u_{\mathrm{EW}}(\mathbf{r})$ and the fit function. While Natoli *et al.* proposed using a sum over many Fourier components for this step, we reached a higher accuracy by performing this calculation in real space, which leads to the usual set of n linear equations,

$$0 = u_{\mathrm{EW},n} - \sum_{|\mathbf{k}|\leq k_c} \tilde{u}_{\mathrm{EW}}(\mathbf{k}) \tilde{f}_n(\mathbf{k}) - \sum_m a_m \left[f_{m,n} - \sum_{|\mathbf{k}|\leq k_c} \tilde{f}_m(\mathbf{k}) \tilde{f}_n(\mathbf{k})\right] \tag{36}$$

with

$$u_{\mathrm{EW},n} = \frac{1}{\Omega}\int d^3\mathbf{r}\, u_{\mathrm{EW}}(\mathbf{r})\, f_m(\mathbf{r}) \quad , \quad f_{n,m} = \frac{1}{\Omega}\int d^3\mathbf{r}\, f_n(\mathbf{r})\, f_m(\mathbf{r}) \quad , \tag{37}$$

and $\tilde{f}_n$ and $\tilde{u}_{\mathrm{EW}}$ being the corresponding Fourier transforms of f_n and u_{EW}. The Fourier coefficients $y_{\mathbf{k}}$ are given by,

$$y_{\mathbf{k}} = \tilde{u}_{\mathrm{EW}}(\mathbf{k}) - \sum_n a_n\, \tilde{f}_n(\mathbf{k}) \ . \tag{38}$$

The background term, C_u, is treated as a $k = 0$ component. In the final step, the real space part,

$$W(|\mathbf{r}|) = \sum_n a_n f_n(|\mathbf{r}|) \ , \tag{39}$$

is conveniently stored on a radial grid and interpolated during PIMC simulations. The same procedure is applied to the τ derivative of the action.

Acknowledgments

E.L. Pollock contributed several important ideas to this manuscript. We also thank Ken Esler, Bernard Bernu, and David Ceperley for useful discussions. We acknowledge support from the U.S. Department of Energy, Grant No. DE-SC0010517.

References

[1] W. M. Foulkes, L. Mitas, R. J. Needs, G. Rajagopal, Rev. Mod. Phys. 73 (2001) 33.
[2] R. P. Feynman, Phys. Rev. 90 (1953) 1116.
[3] R. P. Feynman, Addison-Wesley, Reading, MS, 1972.
[4] E. Pollock, D. M. Ceperley, Phys. Rev. B 30 (1984) 2555.
[5] E. Pollock, D. M. Ceperley, Phys. Rev. B 36 (1987) 8343.
[6] D. M. Ceperley, Rev. Mod. Phys. 67 (1995) 279.
[7] B. Militzer, J. Low Temp. Phys. 139 (2005) 739.
[8] B. Militzer, Phys. Rev. Lett. 97 (2006) 175501.
[9] B. Militzer, Phys. Rev. B 79 (2009) 155105.
[10] B. Militzer, J Phys. A 42 (2009) 214001.
[11] S. X. Hu, B. Militzer, V. N. Goncharov, S. Skupsky, Phys. Rev. Lett. 104 (2010) 235003.
[12] S. X. Hu, B. Militzer, V. N. Goncharov, S. Skupsky, Phys. Rev. B 84 (2011) 224109.
[13] B. Militzer, Phys. Rev. B 87 (2013) 014202.
[14] E. W. Brown, B. K. Clark, J. L. DuBois, D. M. Ceperley, Phys. Rev. Lett. 110 (2013) 146405.
[15] S. X. Hu, V. N. Goncharov, T. R. Boehly, R. L. McCrory, S. Skupsky, L. A. Collins, J. D. Kress, B. Militzer, Physics of Plasmas 22 (2015) 056304.
[16] B. Militzer, R. L. Graham, Journal of Physics and Chemistry of Solids 67 (2006) 2136.
[17] P. Ewald, Ann. Phys. 54 (1917) 557.
[18] L.Hostler, R. H. Pratt, Phys. Rev. Lett. **10** (1963) 469.
[19] C. Pierleoni, D. Ceperley, B. Bernu, W. Magro, Phys. Rev. Lett. 73 (1994) 2145.
[20] W. R. Magro, D. M. Ceperley, C. Pierleoni, B. Bernu, Phys. Rev. Lett. 76 (1996) 1240.
[21] R. G. Storer, J. Math. Phys. 9 (1968) 964.
[22] K. Esler, Ph.D. thesis, University of Illinois at Urbana-Champaign (2006).
[23] V. Natoli, D. M. Ceperley, J. Comp. Phys. 117 (1995) 171–178.
[24] M. Holzmann, B. Bernu, J. Comp. Phys. 206 (2005) 111.
[25] M. Jones, D. Ceperley, Phys. Rev. Lett. 76 (1996) 4572.
[26] B. Militzer, D. M. Ceperley, Phys. Rev. Lett. 85 (2000) 1890.
[27] B. Militzer, D. M. Ceperley, Phys. Rev. E 63 (2001) 066404.
[28] F. H. Zong, C. Lin, D. M. Ceperley, Phys. Rev. E 66 (2002) 036703.
[29] A. D. Klemm, R. G. Storer, Aust. J. Phys. **26** (1973) 43.
[30] K. E. Schmidt, M. A. Lee, Phys. Rev. E 51 (1995) 5495.
[31] J. Shumway, ed. D. P. Landau, S. P. Lewis, and H. B. Schütter, Springer Verlag, Heidelberg, Berlin, 2006.
[32] P. Vieillefosse, J. Stat. Phys. 80 (1994) 561.
[33] E. L. Pollock, Comp. Phys. Comm. 52 (1988) 49.
[34] W. Kolos, L. Wolniewicz, J. Chem. Phys. 41 (1964) 3674.
[35] E. Steiner, Cambdridge University Press, Cambridge, UK, 1976.
[36] B. Militzer, Ph.D. thesis, University of Illinois at Urbana-Champaign (2000).
[37] B. Militzer, D. M. Ceperley, J. D. Kress, J. D. Johnson, L. A. Collins, S. Mazevet, Phys. Rev. Lett. 87 (2001) 275502.
[38] K. P. Driver, B. Militzer, Phys. Rev. Lett. 108 (2012) 115502.
[39] L. X. Benedict, K. P. Driver, S. Hamel, B. Militzer, T. Qi, A. A. Correa, A. Saul, E. Schwegler, Phys. Rev. B 89 (2014) 224109.
[40] K. P. Driver, B. Militzer, Phys. Rev. B 91 (2015) 045103.
[41] K. P. Driver, F. Soubiran, S. Zhang, B. Militzer, J. Chem. Phys. 143 (2015) 164507.
[42] B. Militzer, K. P. Driver, Phys. Rev. Lett. 115 (2015) 176403.
[43] K. P. Driver, B. Militzer, Phys. Rev. B 93 (2016) 064101.
[44] E. L. Pollock, B. Militzer, Phys. Rev. Lett. 92 (2004) 021101.
[45] B. Militzer, E. L. Pollock, Phys. Rev. B 71 (2005) 134303.
[46] M. Allen, D. Tildesley, Oxford University Press, New York, 1987.